JOURNAL OF GEOPHYSICAL RESEARCH, VOL. 112, A06307, doi:10.1029/2007JA012250, 2007

An analysis of the scale heights in the lower topside ionosphere based on the Arecibo incoherent scatter radar measurements

Libo Liu,[1] Huijun Le,[1] Weixing Wan,[1] Mike P. Sulzer,[2] Jiuhou Lei,[3] and Man-Lian Zhang[1]

Received 2 January 2007; revised 23 February 2007; accepted 6 March 2007; published 12 June 2007.

[1] We statistically analyze the ionospheric scale heights in the lower topside ionosphere based on the electron density (N_e) and temperature profiles observed from the incoherent scatter radar (ISR) at Arecibo (293.2°E, 18.3°N), Puerto Rico. In this study, a database containing the Arecibo ISR observations from 1966 to 2002 has been used in order to investigate the diurnal and seasonal variations and solar activity dependences of the vertical scale height (VSH), which is deduced from the electron concentration profiles defined as the value of $-dh/d(\ln(N_e))$, and the effective scale height (H_m), which is defined as the scale height in the Chapman-α function to approximate the N_e profiles. As a measure of the slope of the height profiles of the topside electron density, the derived VSH and H_m show marked diurnal and seasonal variations and solar activity dependences. Their features are discussed in terms of thermal structures in the lower topside ionosphere. We also investigate the quantitative relationships between H_m, VSH, and plasma scale height (H_p) over Arecibo. The similarities and differences in these scale heights are discussed. Results suggest that both the contributions from topside temperature structure and diffusion processes can also greatly control VSH and H_m through changing the profile shape.

Citation: Liu, L., H. Le, W. Wan, M. P. Sulzer, J. Lei, and M.-L. Zhang (2007), An analysis of the scale heights in the lower topside ionosphere based on the Arecibo incoherent scatter radar measurements, *J. Geophys. Res.*, *112*, A06307, doi:10.1029/2007JA012250.

1. Introduction

[2] Knowledge of the spatial distribution of electron number densities or concentrations (N_e) in the ionosphere, especially the height profile $N_e(h)$, is very important for ionospheric scientific studies and empirical modelings as well as practical applications. During the past decades, many mathematical functions, such as the Chapman, exponential, parabolic, and Epstein functions, have been proposed to describe the ionospheric height profiles [e.g., *Bilitza*, 2001; *Bilitza et al.*, 2006; *Booker*, 1977; *Rawer et al.*, 1985; *Rawer*, 1988; *Di Giovanni and Radicella*, 1990; *Stankov et al.*, 2003, 2007]. It is evident that the scale height is an inherent parameter in these ionospheric profile functions [*Stankov et al.*, 2003; *Belehaki et al.*, 2006]. The scale height is one of the important ionospheric characteristics, due to both a measure of the shape of the electron density profile and its intrinsic connection to the ionospheric dynamics, plasma thermal structure and compositions [*Luan et al.*, 2006; *Stankov and Jakowski*, 2006b; *Webb et al.*, 2006]. By studying the behavior of the ionospheric scale heights, we may be capable of answering many open questions in the ionospheric physics, particularly those related to the ionosphere composition and dynamics [e.g., *Liu et al.*, 2004; *Luan et al.*, 2006]. However, the knowledge of the behavior of ionospheric scale heights remains insufficient, especially in the topside ionosphere.

[3] Moreover, it should be mentioned that there are various definitions of the scale heights in published literatures. In order to facilitate description, we adopt the following definitions. The plasma scale height (H_p) is defined as $H_p = k_b T_p / m_i g$, where k_b is the Boltzmann constant, g is the acceleration due to gravity, m_i is the ion mass, and T_p is the plasma temperature, equal to $T_i + T_e$, where T_i and T_e are the ion and electron temperatures. The vertical scale height (VSH) is generally defined as the value of $-dh/d(\ln(N_e))$, relating to the gradient of the measured N_e profiles [*Kutiev et al.*, 2006]. The effective scale height (H_m) is defined as the scale height in fitting the N_e profiles with the Chapman-α function. While H_p is subject to theoretical consideration, VSH and H_m are frequently used in various practical applications [e.g., *Huang and Reinisch*, 1996; *Kutiev et al.*, 2006; *Reinisch et al.*, 2004; *Stankov et al.*, 2003]. Strictly speaking, VSH and H_m virtually are the distribution heights of electron profiles, measuring the altitudinal dependence of the ionospheric electron densities.

[4] The scale heights in the bottomside ionosphere are relatively easy to be deduced from ground-based ionosonde and other measurements. In contrast, the topside scale heights are derived from the incoherent scatter radar (ISR)

[1]Institute of Geology and Geophysics, Chinese Academy of Sciences, Beijing, China.
[2]Arecibo Observatory, National Astronomy and Ionosphere Center, Cornell University, Arecibo, PR, USA.
[3]High Altitude Observatory, National Center for Atmospheric Research, Boulder, Colorado, USA.

0148-0227/07/2007JA012250$09.00

measurements, topside sounders, and radio occultation measurements. For example, *Kutiev et al.* [2006] have identified the lowest gradient of the Ne profile as O^+ scale height from topside ionosondes and first applied it to a scale height model. *Kutiev and Marinov* [2007] reported new progress on the scale height modeling. Moreover, *Stankov and Jakowski* [2006b] conducted an analysis on the topside ionospheric scale height, which is retrieved from radio occultation measurements. Furthermore, *Belehaki et al.* [2006] made a comparison of the topside ionosphere scale height determined by profiles from topside sounders and bottomside digisonde.

[5] Recently, *Huang and Reinisch* [2001] and *Reinisch and Huang* [2004] introduced a technique to extrapolate the topside ionosphere based on the information from ground-based ionograms. They approximated $N_e(h)$ around and above the F2 layer peak (h_mF_2) by a Chapman-α function with an effective scale height (H_m) determined at h_mF_2. The ionogram-derived H_m is a kind of measure of the slope of the electron density profiles in the topside ionosphere. *Liu et al.* [2006a] statistically investigated the diurnal, seasonal, and solar activity variations of H_m at Wuhan (114.4°E, 30.6°N). *Zhang et al.* [2006] reported the diurnal and seasonal variations of H_m over Hainan (109.0°E, 19.4°N). Furthermore, *Lei et al.* [2005] investigated the seasonal and solar activity features of H_m derived from the Millstone Hill ISR observations.

[6] However, up to now, few works investigate and discuss the similarities and differences in these scale heights. Fortunately, the accumulated ISR databases [e.g., *Zhang et al.*, 2004, 2005; *Tepley*, 1997; *Isham et al.*, 2000], topside sounders [*Bilitza et al.*, 2006], and radio occultation measurements, which provide an extremely valuable data source for addressing this issue, are now available.

[7] In this paper, we conduct a statistical analysis on the diurnal, seasonal, and solar cycle variations of H_m and VSH during 1966–2002 from the ISR measurements at Arecibo (293.2°E, 18.3°N; geomagnetic latitude 30°), Puerto Rico. The second objective of this analysis is to investigate the quantitative relationships between VSH versus H_m and VSH versus H_p over Arecibo.

2. Data Source and Analysis

[8] The incoherent scatter radar (ISR) is a powerful technique capable of simultaneously measuring the range-resolved ionospheric and atmospheric parameters [e.g., *Gordon*, 1964; *Evans*, 1969; *Zhou and Sulzer*, 1997; *Isham et al.*, 2000; *Zhang et al.*, 2004], including electron densities as well as plasma drift and temperature profiles, from the lower ionosphere up to the topside ionosphere. The reader is referred to the works of *Tepley* [1997] and *Isham et al.* [2000] for detail information on the Arecibo ISR observations and *Zhang et al.* [2004, 2005] and *Luan et al.* [2006] for the ISR database description.

[9] In the present analysis, we use the ISR data set measured over Arecibo from 1966 to 2002, which are archived in the National Center for Atmospheric Research (NCAR) Coupling, Energetics, and Dynamics of Atmospheric Regions (CEDAR) database. We analyze all available data without specifying the measurement modes. These data have a typical altitude resolution of about 23 km prior to 1985 and 37 km in subsequent years. After removing bad points, the median ISR N_e, T_e, and T_i profiles obtained within every 30-minute interval every day are used for our analysis. We thus have more than 16,000 mean profiles from more than 90,000 raw N_e profiles in the Arecibo ISR database. Now we fit every median N_e profile within 160–600 km using a Chapman-α function as described in the work of *Lei et al.* [2005] but with a scale height H_m independent of altitude. Thus the peak electron density (N_mF_2), its height (h_mF_2), and H_m are determined from the -least squares fitting procedure. Good agreement prevails in most cases, and we discard these profiles when significant deviations may occur under extreme conditions although these profiles may represent the actual situations. On the other hand, the values of VSH are obtained from the median ISR N_e profiles through searching for the lowest value of $-dh/d(\ln(N_e))$ at the lower topside. The curvature of the electron density profile does not allow the determination to begin from the F layer peak so it starts from an altitude about 37 km above the peak. Our derivation of VSH is similar to the methods presented by *Kutiev et al.* [2006] in analyzing topside ionosonde measurements and by *Stankov and Jakowski* [2006a, 2006b] in analyzing radio occultation measurements. At the same time, H_p and the altitude gradients of T_e, and T_i (dT_e/dh and dT_i/dh) at an altitude of 60 km above the F_2 peak are also evaluated from the observed T_i and T_e profiles when they are available.

[10] In this study, $P = (F_{107} + F_{107A}) / 2$ (in units of 10^{-22} W·m^{-2}·Hz^{-1}) is used as the solar activity proxy. Here F_{107} is the 10.7-cm solar flux index on the current day and F_{107A} is the 81-day average of F_{107} centered on the current day. It was indicated by *Liu et al.* [2006b] that *P*, which was adopted by *Hinteregger et al.* [1981] and

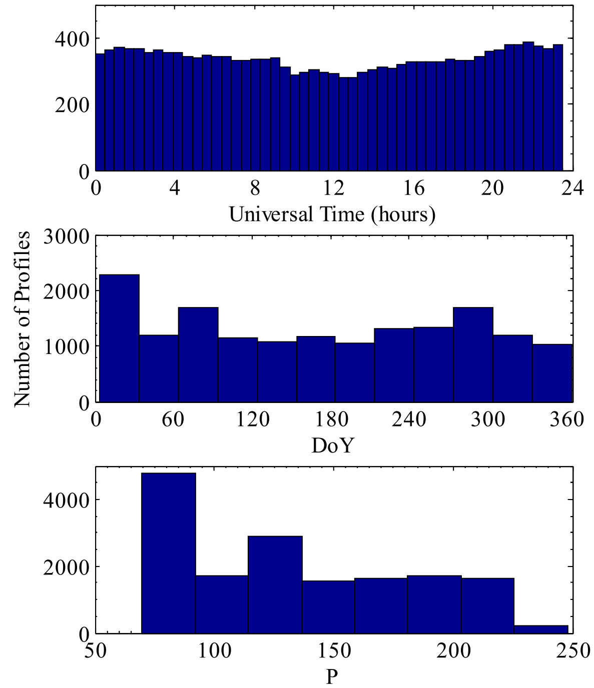

Figure 1. The distributions of number of mean profiles as a function of (top) universal time, (middle) the day number of year, and (bottom) *P* (in units of 10^{-22} W·m^{-2}·Hz^{-1}).

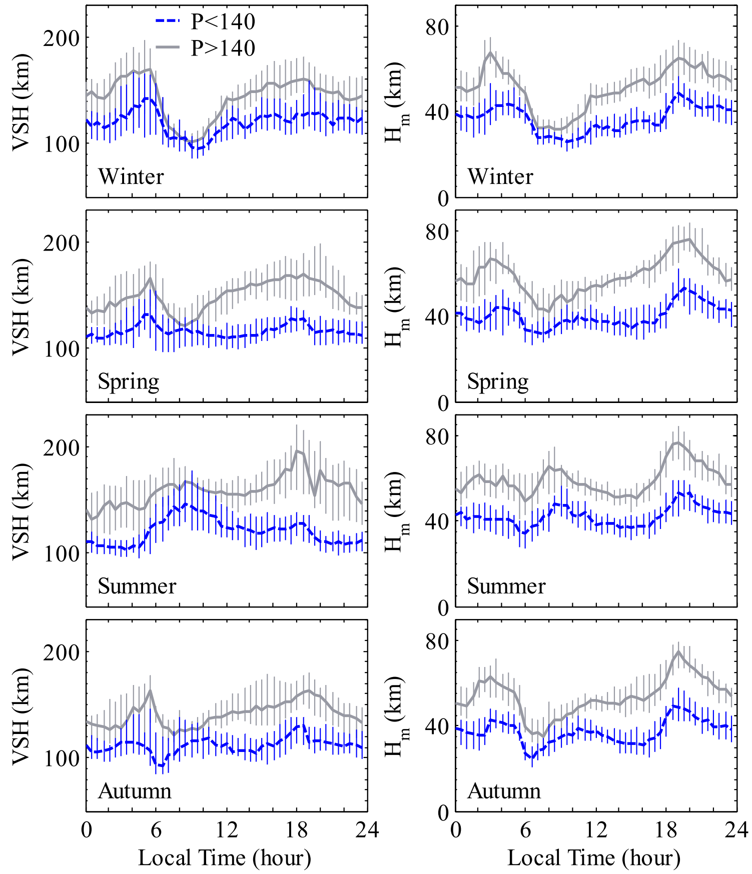

Figure 2. Diurnal and seasonal variations of (left) VSH and (right) H_m for two solar activity levels (P > 140 and P < 140 × 10^{-22} W·m^{-2}·Hz^{-1}). Here $P = (F_{107} + F_{107A}) / 2$, where F_{107A} is the 81-day running mean of daily F_{107} index. Lines with bars represent the half-hourly median values of VSH and H_m and the corresponding upper and lower quartiles, respectively.

Richards et al. [1994], can better represent the intensities of solar extreme ultraviolet (EUV) fluxes than F_{107}. Furthermore, *Zhang et al.* [2004] found that the correlations of Millstone Hill N_e, T_e, and T_i with different F_{107} values (for the current day and some days earlier) are really not significantly different. Thus we opt to the current day's P for the solar activity proxy in the following statistical analysis.

[11] Figure 1 shows the distributions of the number of mean profiles as a function of P, day of year (DoY), and universal time (UT), indicating that the data are uniformly distributed in UT and DoY. The number of mean profiles available for P < 140 is comparable to that for P > 140, thus we split data into two categories at solar activity levels with P > 140 and P < 140, respectively.

3. Results

3.1. Seasonal and Solar Activity Variability of VSH and H_m Over Arecibo

[12] VSH and H_m over Arecibo are derived from the median ISR N_e profiles within 30-minute intervals for each day when measured profiles are available. Figure 2 shows the median values of VSH and H_m, which are binned according to universal time at two solar activity levels (P > 140 and P < 140, respectively) in four seasons. Vertical bars in Figure 2 depict the corresponding upper and lower quartiles values to show the deviations from the averages.

[13] Over Arecibo, as illustrated in Figure 2, VSH and H_m have distinct diurnal variations in four seasons. The median values of VSH and H_m are generally higher for P > 140 than that for P < 140; that is, VSH and H_m have solar activity dependency. There are two peaks in the diurnal variations of VSH and H_m, one in the early morning and another one located in the afternoon to the evening sector. After the morning peak, VSH and H_m descend. Next, they approach a minimum at 6–8 LT and rise again, reaching maximum in the evening. Later they tend to decrease again till midnight. In summer, the first peak shifts to later time. Moreover, the sunrise descent is marked in spring and autumn and most intensely in winter, while the trend during this time is opposite in summer. In the morning, the values of VSH and H_m are highest in summer and lowest in winter; while at rest time, the seasonal variation is less distinct.

[14] For the daytime, the yearly variations of VSH and H_m over Arecibo (higher values in summer) are consistent with the radio occultation results of *Stankov and Jakowski* [2006b]. It should be noted that the data sources are from different measuring techniques and the scale height presented in Figure 16 in the work of Stankov and Jakowski is actually H, having values half of this of ISR VSH. However,

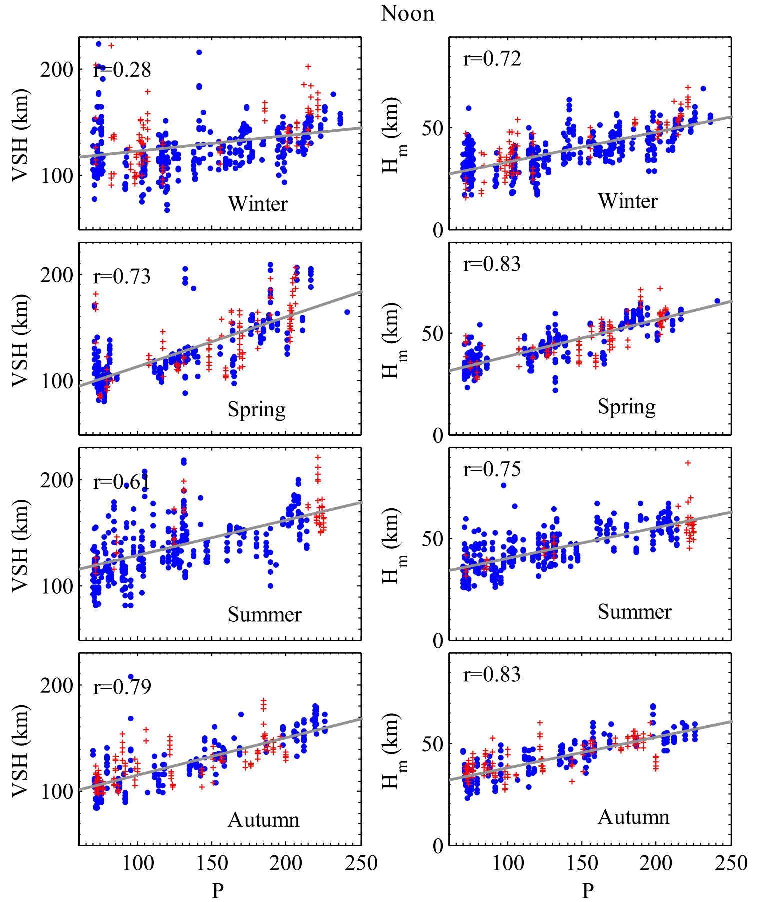

Figure 3. Scatterplots of (left) VSH and (right) H_m versus P (10^{-22} W·m^{-2}·Hz^{-1}) around local noon in four seasons. The solid lines show the trend of the linear regression.

in the study of *Liu et al.* [2006a], the features in VSH and H_m are not as distinct as the ionogram derived H_m over Wuhan and other locations. Moreover, a distinct yearly annual variation is presented in global H_m with a maximum in summer during the daytime. The discrepancies may possibly be due to different data sources. Furthermore, the ionogram derived H_m in the work of *Liu et al.* [2006a] is estimated only from the bottomside profiles, while here we use ISR N_e profiles with both the bottomside and topside information.

[15] The geomagnetic disturbance effects on the ionosphere are well known to be complicated and stochastic [e.g., *Liu et al.*, 2006a; *Kutiev et al.*, 2006; *Stankov and Jakowski*, 2006b]. The geomagnetical activity dependences of VSH and H_m at Arecibo have been statistically investigated with the planetary geomagnetical indices, 3-hour kp and ap, and the daily Kp and Ap. Similar to the geomagnetical activity dependences of H_m over Wuhan [*Liu et al.*, 2006a], although individual VSH and H_m may greatly deviate from the average pattern under disturbed situations, the statistical relationship between these geomagnetical indices and VSH or H_m are not significant and with a low correlation coefficient (figures not shown here). This feature can also be inferred from Figures 3 and 4; the trend of data (with plus symbols (+)) under geomagnetically active conditions (AP > 20) is similar to that (with dot symbols '·') under quiet to moderate conditions (AP < 20). It implies complicated dependences of VSH and H_m on geomagnetic activity and insignificant differences in the median values of VSH and H_m whether or not the geomagnetic conditions take into account. Thus, we can ignore the geomagnetical activity effects in our further statistical analysis.

[16] Figure 3 shows the solar activity dependences of VSH and H_m around local noon and Figure 4 for VSH and H_m at midnight in four seasons. In these figures, data under AP > 20 are plotted with plus (+) symbols. It also indicates that possible influences of geomagnetic activities do not systemically deviated the solar activity dependences of VSH and H_m. An evident feature illustrated in Figures 3 and 4 is that the overall trend of VSH and H_m linearly increases with respect to P. With increasing P, both VSH and H_m evidently tend to be higher. This feature is more significant than that derived from radio occultation measurements [*Stankov and Jakowski*, 2006b]. Another very interesting feature is that H_m shows a stronger correlation with P than VSH; for example, winter noon r = 0.28 for VSH and r = 0.72 for H_m (see Figures 3 and 4).

[17] In order to quantitatively study the solar activity dependences of VSH and H_m, we calculate the slope or the increase rate of VSH and H_m with the solar flux index P, dVSH/dP and dH_m/dP. dVSH/dP and dH_m/dP is a measure of the response of VSH and H_m to solar activity. Figure 5 demonstrates the values of calculated dVSH/dP and dH_m/dP against local time in four seasons. It is seen that the solar activity sensitivities of VSH and H_m also undergo appre-

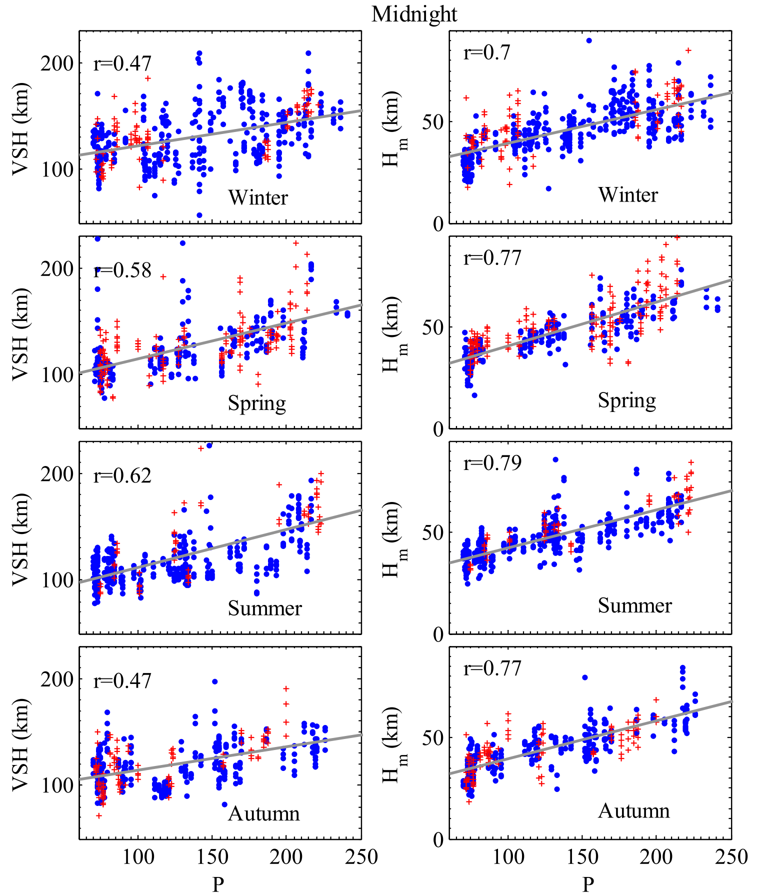

Figure 4. Same as Figure 3, but for local midnight.

ciable local time changes. The feature of both rates is generally similar with each other; that is, the values of both dVSH/dP and dH_m/dP present a post-midnight increase, follow a sharp decrease, and reach a minimum in the morning (around 12 UT). After the minimum, the solar activity responses of VSH and H_m become more effective again. dH_m/dP is generally higher in equinoxes and summer than in winter, which is similar to that over Millstone Hill [*Lei et al.*, 2005].

3.2. Diurnal and Solar Activity Variability of H_p Over Arecibo

[18] Figure 6 plots the diurnal variations of H_p over Arecibo in a similar style of Figure 2 for VSH and H_m. There are distinct diurnal variations in H_p for four seasons with a higher value during the daytime than at nighttime. A particular feature of H_p is the dawn and afternoon peaks with a valley around noon, the morning peak being stronger.

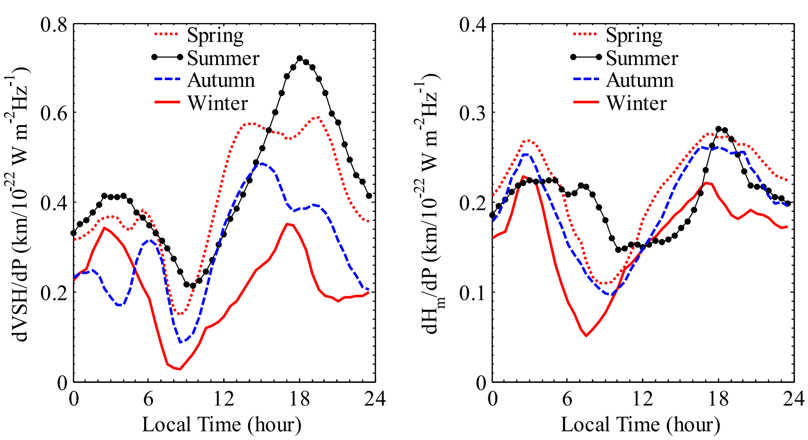

Figure 5. Diurnal variations of the rates of VSH and H_m increase with P (10^{-22} W·m^{-2}·Hz^{-1}) in four seasons.

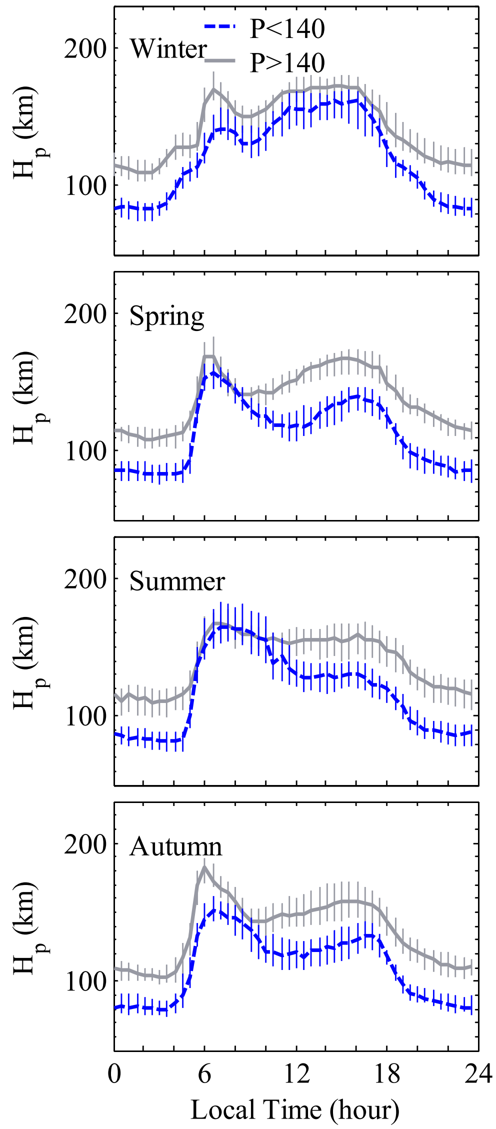

Figure 6. Diurnal and seasonal variations of plasma scale height (H_p) for two solar activity levels ($P > 140$ and $P < 140$). Here $P = (F_{107} + F_{107A}) / 2$, where F_{107A} is the 81-day running mean of daily F_{107} index. Lines with bars represent the half-hourly median values of VSH and H_m and the corresponding upper and lower quartiles, respectively.

[19] According to the definition, H_p is directly proportional to the plasma temperature. As far as the temperatures experience significant changes H_p also presents similar variations. Higher T_e and T_i imply a larger scale height. The significant morning rise in electron and ion temperatures in the F layer, known as morning overshot, is an important feature of the diurnal variation, as reported previously from satellite measurements [*Bhuyan et al.*, 2006; *Oyama et al.*, 1996; *Sharma et al.*, 2005] and ISR analysis [e.g., *MacPherson et al.*, 1998; *Zhang et al.*, 2004]. This feature is also presented in the first peak in H_p, which is consistent with that of VSH and H_m, except much late in VSH and H_m in summer. Overall, our results suggest the diurnal behaviors of VSH and H_m are much more complex than that of H_p.

[20] The behavior of the electron temperature is dependent on photoelectron heating and is closely coupled to the electron density [*Lei et al.*, 2007]. The morning temperature enhancement is due to photoelectron heating [e.g., *Oyama et al.*, 1996]. The afternoon enhancement comes from the balance of heating and cooling. In contrast, the particular noon valley results from the competition between the electron heating and cooling processes in the thermal balance. Although near noon the electron heating has its greatest value, its effect on the thermal balance is more than offset by the electron cooling resulting from the higher noontime electron densities [*Su et al.*, 1995]. As a result, a lower T_e appears around noon when N_e is high and the electron cooling is strong. At sunset, T_e decreases [*MacPherson et al.*, 1998]. As a result of this cooling, H_p has a lower value during the nighttime.

[21] Except at a narrow local time interval before local noon in summer and spring, the median value of H_p is generally larger for $P > 140$ than that for $P < 140$; that is, H_p presents a similar sense as VSH and H_m in solar activity dependency.

[22] Figure 7 illustrates the solar activity dependencies of noon and midnight H_p over Arecibo in a similar style of Figures 3 and 4 for VSH and H_m. In the figure, data under AP > 20 are also plotted with plus (+) symbols. It further indicates that possible influences of geomagnetic activities do not systemically deviated from the solar activity dependences. The overall trend of H_p also linearly increases with respect to P, being a strong correlation at night and equinox noon and weaker around noon in summer and winter.

3.3. The Correlation of VSH Versus H_m and VSH Versus H_p

[23] Scatterplots illustrate in Figure 8 show the relationship between VSH and H_m over Arecibo. The left panels of Figure 8 are for the values around noon and the right panels for midnight, respectively. In general, VSH shows a moderate positive correlation with H_m with a higher correlation coefficient during the daytime than that at night.

[24] VSH is expected to be twice of H_m under diffusive equilibrium. However, according to the regression analysis, VSH exhibit a linear relation with H_m with a ratio (VSH to H_m) varied from 1.4 to 6. The relationship between VSH and H_m can be quantified using a linear expression, illustrating by the solid line. A dashed line of VSH = $2H_m$ in Figures 8 indicates how much the two scale heights deviate. The corresponding regression equation is listed at each panel in Figure 8. Coefficients indicate that the relation between VSH and H_m vary with local time and season.

[25] We have also investigated the quantitative relationships between VSH and H_p over Arecibo. Figure 9 shows the relationship between VSH and H_p over Arecibo. The left panels of Figure 9 are for the values around noon and the right panels for midnight, respectively. The local time dependence of the correlations between VSH and H_m and between VSH and H_p is shown in the right panels of Figure 10. In general, VSH shows a moderate positive correlation with H_m or with H_p with a high correlation coefficient. An exception is found at 05–07 LT, being a weaker correlation at that period.

[26] To resolve the local time dependence of the quantitative relationships between VSH versus H_m and VSH

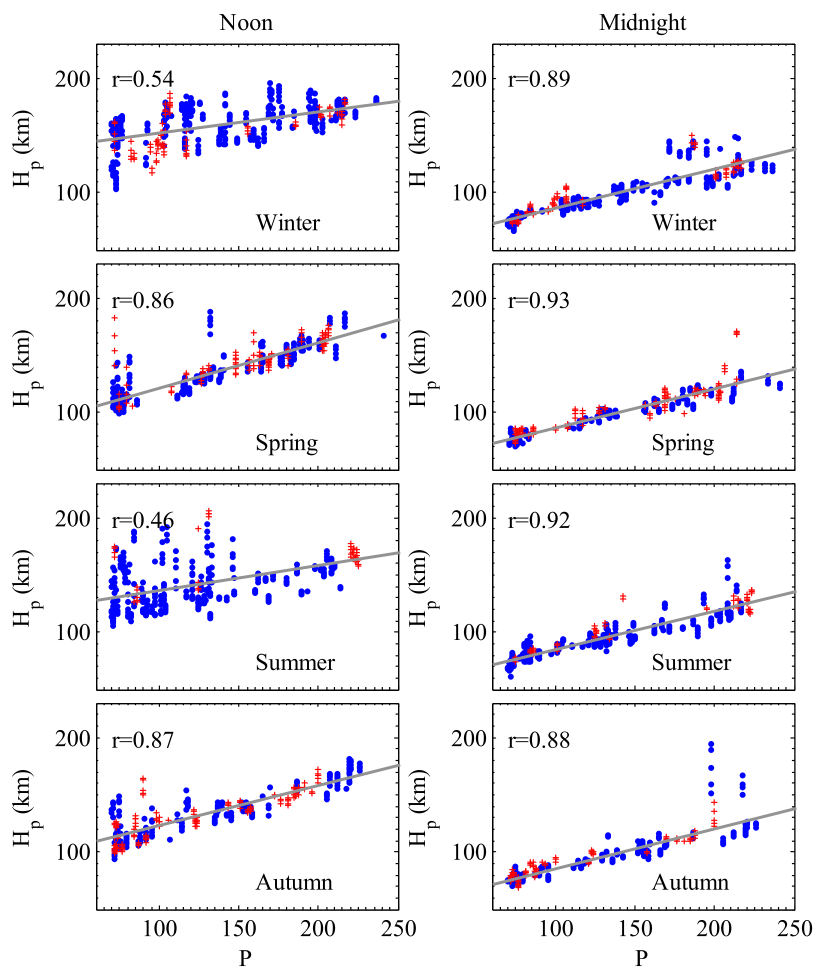

Figure 7. Scatterplots of H_p versus P (in units of 10^{-22} W·m^{-2}·Hz^{-1}) around (left) local noon and (right) midnight in four seasons. The solid lines show the trend of the linear regression. The red points with symbol (+) are for data with Ap > 20 and the dotted points are for Ap < 20.

versus H_p, we present the ratios of VSH to H_m and VSH to H_p over Arecibo in the left panels of Figure 10. Lines with bars represent the moving median values of the ratios and the corresponding upper and lower quartiles within 2 hours, respectively. The median ratios of VSH to H_m have values about 3.2 by daytime and 2.7 at night; those of VSH to H_p have values about 0.9 by daytime and 1.3 at night.

4. Discussion

[27] As mentioned above, the scale height is theoretically defined as $H = k_b T/mg$, where T is the temperature and m is the mass. According to this definition, the plasma scale height, H_p, is defined as $H_p = k_b T_p/m_i g$. However, in general, H_p is most difficult to obtain and not directly related to the N_e profiles. In practice, the effective scale height, H_m, is a scale height in the Chapman-α function to fitting the N_e profile. Moreover, the vertical scale height, VSH, is generally defined as the value of $-dh/d(\ln(N_e))$, relating to the gradient of the measured N_e profiles [e.g., *Kutiev et al.*, 2006]. VSH in this report is approximately deduced as the lowest value in the topside ionosphere as *Kutiev et al.* [2006] and *Stankov and Jakowski* [2006b].

[28] Considering only the vertical drift and ignoring the horizontal gradient in the ionosphere, *Rishbeth and Garriott* [1969] deduced their equation (431) based on ion and electron momentum equations. According to the equation (431) of *Rishbeth and Garriott* [1969], we have

$$\frac{1}{\mathrm{VSH}} = -\frac{1}{N_e}\frac{dN_e}{dh} = \frac{1}{H_p} + \frac{m_i \nu_{in} W_D}{k_b(T_i + T_e)} + \frac{d(T_i + T_e)/dh}{(T_i + T_e)}. \quad (1)$$

Here ν_{in} is the collision frequency of ions with neutrals and W_D is the vertical diffusion velocity of ions.

[29] Equation (1) illustrates the relationship between VSH and H_p under the controls of diffusion and gradient terms. According to equation (1), there are many factors that act to control VSH. VSH equals to H_p, if the topside ionosphere is in a state dominated by diffusive equilibrium ($W_D = 0$) and the altitude gradient of the thermal structure can be ignored. However, the median ratios of VSH to H_p are about 0.9 by daytime and 1.3 at night. As we know, the transport processes become more important in the topside ionosphere. The dynamics in the topside ionosphere is dominated by plasma diffusion, in which the topside thermal structure, the ion composition, field-aligned fluxes, and ion-neutral drag

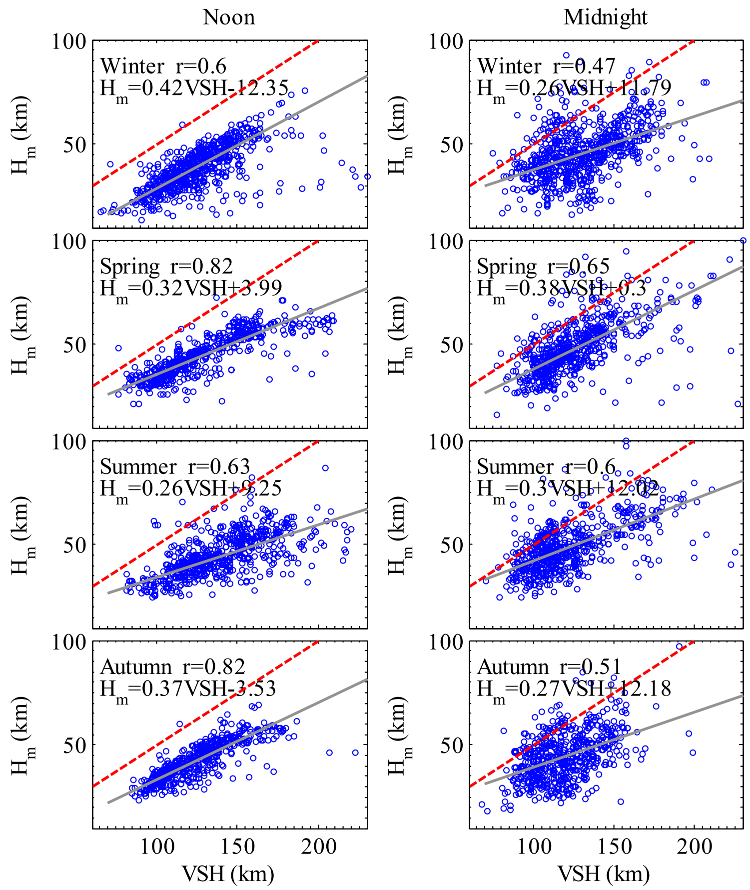

Figure 8. Scatterplots of VSH versus H_m at Arecibo around local (left) noon and (right) midnight during 1966–2002 in four seasons. The solid lines show the trend of the linear regression and the dashed lines show VSH = $2H_m$. In each panel, the equation lists the fitted linear relationship between VSH and H_m and r is the corresponding correlation coefficient.

motions caused by neutral winds. For example, investigations indicated that the movement of the ionosphere due to neutral winds may be an important cause of the variations of topside ionosphere [*MacPherson et al.*, 1998; *Oyama et al.*, 1996; *Zhang et al.*, 2005], and consequently the profile shape of the topside ionosphere is modified.

[30] As indicated by equation (1), the topside temperature structure will influence the shape of the electron profile. Figure 11 shows the diurnal variation of $\frac{dT_i/dh + dT_e/dh}{(T_i+T_e)}$ in four seasons for two solar activity levels ($P > 140$ and $P < 140$). As seen in Figure 11, there are significant altitude gradients (dT_e/dh and dT_i/dh) in the topside temperature profiles at the time interval from sunrise to sunset, while it is negligible during night. This point can also be inferred from Figure 4 in the work of *Lei et al.* [2007]. Assume with a given H_p and other factors be constant, higher $\frac{dT_i/dh + dT_e/dh}{(T_i+T_e)}$ will tend to decrease VSH, according to equation (1). This is consistent with the diurnal features illustrated in Figure 10 and Figure 11.

[31] Besides the contributions from the topside temperature structure, diffusion process ($W_D \neq 0$) can also greatly influence the shape of topside profile. According to *Luan et al.* [2006], the effect of diffusion tends to cause the shape factor increase by day and decrease at night. It is equivalent to that the scale height tends to decrease by day and increase at night. Therefore the combined effects cause that, in general, VSH will deviate from H_p or the plasma temperature.

[32] On the other hand, assume the N_e profiles around the F-region can be reasonably approximated by the Chapman-type function,

$$N_e(h) = N_mF_2 \exp\{f[1 - z - \exp(-z)]\},\quad z = (h - h_mF_2)/H_m, \tag{2}$$

we have

$$\frac{1}{\mathrm{VSH}} = \frac{f}{H_m}(1 - e^{-z}) \tag{3}$$

Where f is the shape factor [see *Luan et al.*, 2006].

[33] When discussing the differences between VSH and H_m, equation (3) indicates that VSH and H_m is related with the profile factor f. VSH is roughly expected twice H_m, which is assumed in many previous published papers. For Chapman-α profile, $f = 0.5$. Above h_mF_2, the formula (if take $f = 0.5$ and assume $z \gg 1$) provides a density gradient of $2H_m$. However, *Luan et al.* [2006] found that, over Arecibo, f varies from 0.35 to 0.75 with a daytime maximum, a nearly constant nighttime value, and a deep

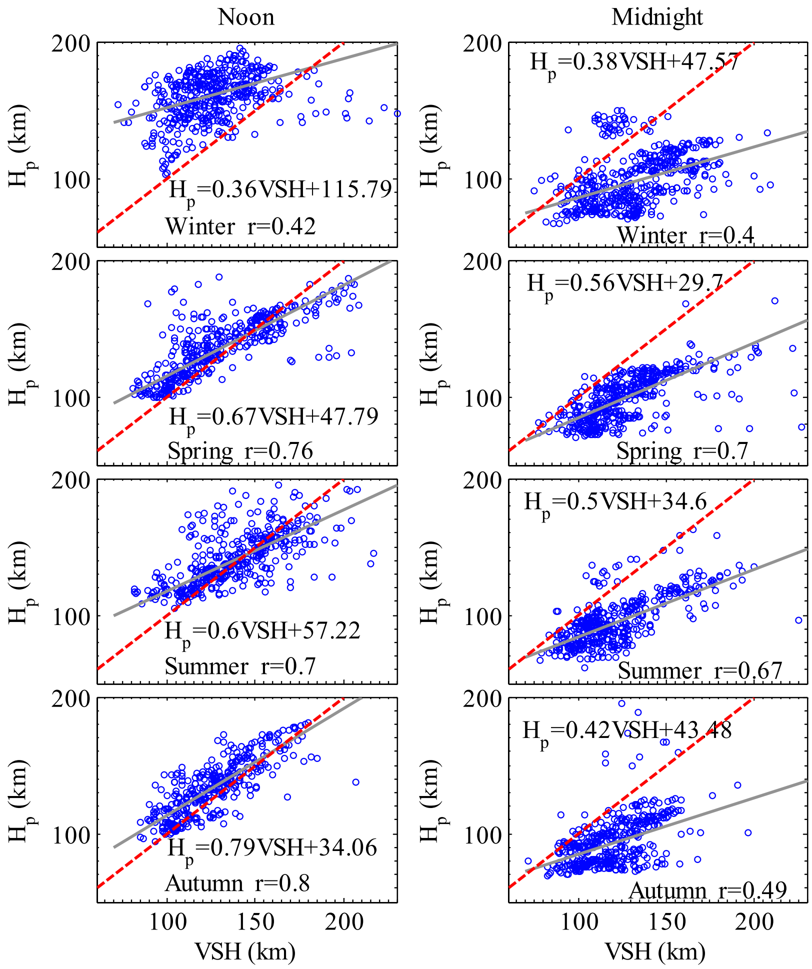

Figure 9. Scatterplots of VSH versus H_p at Arecibo around local (left) noon and (right) midnight during 1966–2002 in four seasons. The solid lines show the trend of the linear regression and the dashed lines show VSH = H_m. In each panel, the equation lists the fitted linear relationship between VSH and H_p and r is the corresponding correlation coefficient.

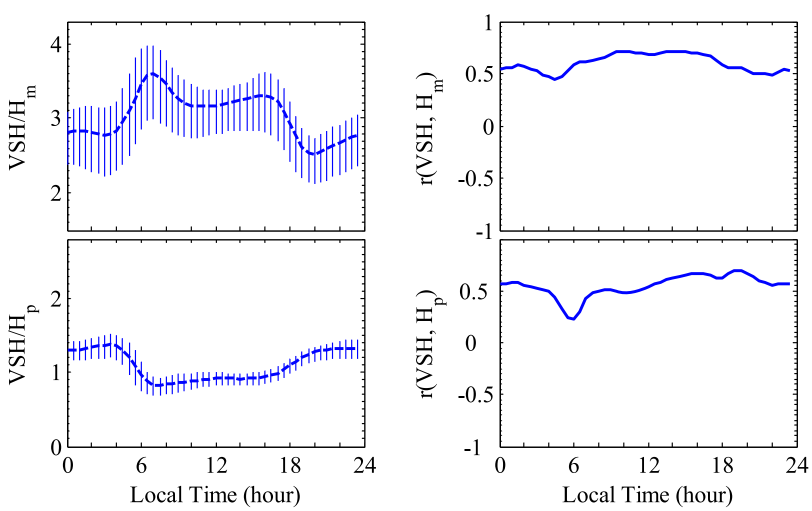

Figure 10. (Left) Diurnal variations of the ratios of (top) VSH to H_m and (bottom) VSH to H_p. Lines with bars respectively represent the median values of the ratios and the corresponding upper and lower quartiles within 2 hours. (Right) Diurnal variations of the correlation coefficients of (top) VSH to H_m and (bottom) VSH to H_p.

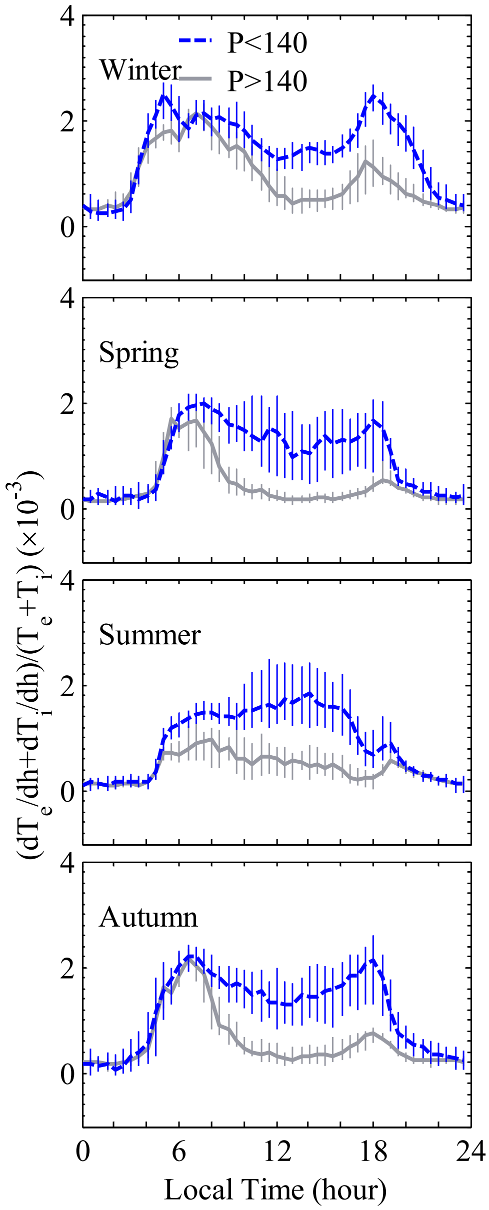

Figure 11. Same as Figure 6, but for $\frac{\mathrm{d}T_\mathrm{i}/\mathrm{d}h+\mathrm{d}T_\mathrm{e}/\mathrm{d}h}{(T_\mathrm{i}+T_\mathrm{e})}$.

morning minimum. The deep morning minimum feature in the profile factor *f* is consistent with the morning peak in the ratio of VSH to H_m (see the top-left panel of Figure 10). Moreover, the height where VSH is determined depends on the composition change in the topside ionosphere; that is, the relative abundance of hydrogen ions H^+, or equivalent to the upper transition level, is a significant factor affecting the topside density profile [*Stankov and Jakowski*, 2006a, 2006b]. The upper transition level increases with increasing *P*. So the height where VSH is determined changes with *P*. Large downward fluxes of H^+ in the morning hours can decrease the upper transition levels [*Jayachandran et al.*, 2004], thereby decreasing VSH and H_m. Therefore it is easily understood that the ratio of VSH to H_m also change from 3.2 by daytime to 2.7 at night.

[34] In addition, as a measure of the slope of the topside electron number density profile, H_m is also a measure of the topside thickness of the ionosphere [*Gulyaeva*, 2007], and the slab thickness [e.g., *Goodwin et al.*, 1995; *Jayachandran et al.*, 2004] according to the statistical study of *Huang and Reinisch* [2001] on $N_\mathrm{m}F_2$, TEC and H_m, although the values of H_m, the topside thickness, and the slab thickness may be different from each other. Moreover, since the Chapman function can well describe the distribution of the electron density of the topside ionosphere not far away from the F layer peak, VSH and H_m should have significant values for future empirical applications [*Stankov et al.*, 2003].

5. Summary

[35] This paper investigates the diurnal, seasonal, and solar activity variations of the topside ionospheric scale heights observed at Arecibo. The main results are summarized as follows: This statistical analysis identifies a clear and unambiguous solar activity pattern of VSH, H_m, and H_p over Arecibo; that is, these scale heights tend to a higher value with increasing solar flux. Moreover, VSH and H_m at Arecibo have appreciable diurnal, seasonal variations. The diurnal behaviors of seasonal median VSH and H_m under both solar activities are found to be similar. Median values of H_m are highest in summer and lowest in winter during the daytime. At nighttime, H_m exhibits a much weaker seasonal variation. Overall, our results suggest the diurnal behaviors of VSH and H_m are much more complex than that of H_p. VSH is not so tightly correlated with the plasma temperature or H_p as originally expected.

[36] The similarities and differences in these scale heights are discussed in terms of thermal structures in the lower topside ionosphere. Combined investigations made by *Luan et al.* [2006] and our results suggest that both the contributions from topside temperature structure and diffusion processes can greatly control VSH and H_m through changing the profile shape.

[37] **Acknowledgments.** The authors thank two referees for their valuable suggestions to the paper. This study made use of the NCAR CEDAR database which is supported by the National Science Foundation of USA. The Arecibo Observatory is operated by Cornell University under an agreement with the National Science Foundation of USA. This research was supported by National Natural Science Foundation of China (40674090, 40636032), the KIP Pilot Project (kzcx3-sw-144) of Chinese Academy of Sciences, and National Important Basic Research Project (2006CB806306).

[38] Wolfgang Baumjohann thanks Ivan Kutiev and another reviewer for their assistance in evaluating this paper.

References

Belehaki, A., P. Marinov, I. Kutiev, N. Jakowski, and S. Stankov (2006), Comparison of the topside ionosphere scale height determined by topside sounders model and bottomside digisonde profiles, *Adv. Space Res.*, *37*, 963–966.

Bhuyan, P. K., M. Chamua, P. Subrahmanyam, and S. C. Garg (2006), Effect of solar activity on diurnal and seasonal variations of electron temperature measured by the SROSS C2 over Indian low latitudes, *Adv. Space Res.*, *37*, 885–891.

Bilitza, D. (2001), International reference ionosphere 2000, *Radio Sci.*, *36*(2), 261–275.

Bilitza, D., B. W. Reinisch, S. M. Radicella, S. Pulinets, T. Gulyaeva, and L. Triskova (2006), Improvements of the International reference ionosphere model for the topside electron density profile, *Radio Sci.*, *41*, RS5S15, doi:10.1029/2005RS003370.

Booker, H. G. (1977), Fitting of multi-region ionospheric profiles of electron density by a single analytic function of height, *J. Atmos. Terr. Phys.*, *39*, 619–623.

Di Giovanni, G., and S. M. Radicella (1990), An analytical model of the electron density profile in the ionosphere, *Adv. Space Res.*, *10*(11), 27–30.

Evans, J. V. (1969), Theory and practice of ionosphere study by Thomson scatter radar, *Proc. IEEE*, *57*(4), 496–530.
Goodwin, G. L., J. H. Silby, K. J. W. Lynn, A. M. Breed, and E. A. Essex (1995), GPS satellite measurements: ionospheric slab thickness and total electron content, *J. Atmos. Terr. Phys.*, *57*(14), 1723–1732.
Gordon, W. E. (1964), Arecibo ionospheric observatory, *Science*, *146*, 26–30.
Gulyaeva, T. (2007), Variable coupling between the bottomside and topside thickness of the ionosphere, *J. Atmos. Sol. Terr. Phys.*, doi:10.1016/j.jastp.2006.10.015.
Hinteregger, H. E., K. Fukui, and B. R. Gilson (1981), Observational, reference and model data on solar EUV, from measurements on AE-E, *Geophys. Res. Lett.*, *8*, 1147–1150.
Huang, X., and B. W. Reinisch (1996), Vertical electron profiles from the Digisonde network, *Adv. Space Res.*, *18*(6), 121–129.
Huang, X., and B. W. Reinisch (2001), Vertical electron content from ionograms in real time, *Radio Sci.*, *36*(2), 335–342.
Isham, B., C. A. Tepley, M.P. Sulzer, Q. H. Zhou, M. C. Kelley, J. S. Friedman, and S. A. González (2000), Upper atmospheric observations at the Arecibo Observatory: Examples obtained using new capabilities, *J. Geophys. Res.*, *105*(A8), 18,609–18,637.
Jayachandran, B., T. N. Krishnankutty, and T. L. Gulyaeva (2004), Climatology of ionospheric slab thickness, *Ann. Geophys.*, *22*, 25–33.
Kutiev, I., and P. Marinov (2007), Topside sounder model of scale height and transition height characteristics of the ionosphere, *Adv. Space Res.*, *39*, doi:10.1016/j.asr.2006.06.013.
Kutiev, I. S., P. G. Marinov, and S. Watanabe (2006), Model of topside ionosphere scale height based on topside sounder data, *Adv. Space Res.*, *37*, 943–950.
Lei, J., L. Liu, W. Wan, and S.-R. Zhang (2005), Variations of electron density based on long-term incoherent scatter radar and ionosonde measurements over Millstone Hill, *Radio Sci.*, *40*, RS2008, doi:10.1029/2004RS003106.
Lei, J., R. G. Roble, W. Wang, B. A. Emery, and S.-R. Zhang (2007), Electron temperature climatology at Millstone Hill and Arecibo, *J. Geophys. Res.*, *412*, A02302, doi:10.1029/2006JA012041.
Liu, L., X. Luan, W. Wan, J. Lei, and B. Ning (2004), Solar activity variations of equivalent winds derived from global ionosonde data, *J. Geophys. Res.*, *109*, A12305, doi:10.1029/2004JA010574.
Liu, L., W. Wan, and B. Ning (2006a), A study of the ionogram derived effective scale height around the ionospheric h_mF_2, *Ann. Geophysicae*, *24*(3), 851–860.
Liu, L., W. Wan, B. Ning, O. M. Pirog, and V. I. Kurkin (2006b), Solar activity variations of the ionospheric peak electron density, *J. Geophys. Res.*, *111*, A08304, doi:10.1029/2006JA011598.
Luan, X., L. Liu, W. Wan, J. Lei, S.-R. Zhang, J. M. Holt, and M. P. Sulzer (2006), A study of the shape of the topside electron density profile derived from incoherent scatter radar measurements over Arecibo and Millstone Hill, *Radio Sci.*, *41*, RS4006, doi:10.1029/2005RS003367.
MacPherson, B., S. A. González, G. J. Bailey, R. J. Moffett, and M. P. Sulzer (1998), The effects of meridional neutral winds on the O^+–H^+ transition altitude over Arecibo, *J. Geophys. Res.*, *103*(A12), 29,183–29,198.
Oyama, K.-I., S. Watanabe, Y. Su, T. Takahashi, and K. Hiro (1996), Seasonal, local time, and longitudinal variations of electron temperature at the height of ~600 km in the low latitude region, *Adv. Space Res.*, *18*(6), 269–278.
Rawer, K. (1988), Synthesis of ionospheric electron density profiles with Epstein functions, *Adv. Space Res.*, *8*(4), 191–198.
Rawer, K., D. Bilitza, and T. L. Gulyaeva (1985), New formulas for IRI electron density profile in the topside and middle ionosphere, *Adv. Space Res.*, *5*(7), 3–12.
Reinisch, B. W., and X. Huang (2004), Deducing topside profiles and total electron content from bottomside ionograms, *Adv. Space Res.*, *27*(1), 23–30.
Reinisch, B. W., X. Huang, A. Belehaki, J. Shi, M. Zhang, and R. Ilma (2004), Modeling the IRI topside profile using scale height from ground-based ionosonde measurements, *Adv. Space Res.*, *34*, 2026–2031.
Richards, P. G., J. A. Fennelly, and D. G. Torr (1994), EUVAC: A solar EUV flux model for aeronomic calculations, *J. Geophys. Res.*, *99*(A5), 8981–8992.
Rishbeth, H., and O. K. Garriott (1969), *Introduction to Ionospheric Physics*, 331 pp., Academic Press, New York.
Sharma, D. K., J. Rai, M. Israil, and P. Subrahmanyam (2005), Diurnal, seasonal and longitudinal variations of ionospheric temperatures of the topside F region over the Indian region during solar minimum (1995–1996), *J. Atmos. Sol. Terr. Phys.*, *67*, 269–274.
Stankov, S. M., and N. Jakowski (2006a), Topside plasma scale height retrieved from radio occultation measurements, *Adv. Space Res.*, *37*, 958–962.
Stankov, S. M., and N. Jakowski (2006b), Topside ionospheric scale height analysis and modeling based on radio occultation measurements, *J. Atmos. Sol. Terr. Phys.*, *68*, 134–162.
Stankov, S. M., N. Jakowski, S. Heise, P. Muhtarov, I. Kutiev, and R. Warnant (2003), A new method for reconstruction of the vertical electron density distribution in the upper ionosphere and plasmasphere, *J. Geophys. Res.*, *108*(A5), 1164, doi:10.1029/2002JA009570.
Stankov, S. M., P. Marinov, and I. Kutiev (2007), Comparison of NeQuick, PIM, and TSM model results for the plasma scale and transition heights, *Adv. Space Res.*, *39*, doi:10.1016/j.asr.2006.10.023.
Su, Y. Z., K.-I. Oyama, G. J. Bailey, T. Takashi, and S. Watanabe (1995), Comparison of satellite electron density and temperature measurements at low latitudes with a plasmasphere-ionosphere model, *J. Geophys. Res.*, *100*(A8), 14,591–14,604.
Tepley, C. A. (1997), Current developments at Arecibo for research in the atmospheric sciences at low latitudes, *J. Atmos. Sol. Terr. Phys.*, *57*(13), 1679–1686.
Webb, P. A., R. F. Benson, and J. Grebowsky (2006), Altitude variations of middle-latitude topside ionospheric electron-density profiles, *Adv. Space Res.*, *37*, 951–957.
Zhang, S.-R., J. M. Holt, A. M. Zalucha, and C. Amory-Mazaudier (2004), Midlatitude ionospheric plasma temperature climatology and empirical model based on Saint Santin incoherent scatter radar data from 1966 to 1987, *J. Geophys. Res.*, *109*, A11311, doi:10.1029/2004JA010709.
Zhang, S.-R., J. M. Holt, A. P. van Eyken, M. McCready, C. Amory-Mazaudier, S. Fukao, and M. Sulzer (2005), Ionospheric local model and climatology from long-term databases of multiple incoherent scatter radars, *Geophys. Res. Lett.*, *32*, L20102, doi:10.1029/2005GL023603.
Zhang, M.-L., B. W. Reinisch, J. S. Shi, S. Wu, and X. Wang (2006), Diurnal and seasonal variation of the ionogram-derived scale height at the F2 peak, *Adv. Space Res.*, *37*, 967–971.
Zhou, Q. H., and M. P. Sulzer (1997), Incoherent scatter radar observations of the F-region ionosphere at Arecibo during January 1993, *J. Atmos. Sol. Terr. Phys.*, *59*(17), 2213–2229.

H. Le, L. Liu, and W. Wan, Institute of Geology and Geophysics, Chinese Academy of Sciences, Beijing 100029, China. (lehj@mail.iggcas.ac.cn; liul@mail.iggcas.ac.cn; wanw@mail.iggcas.ac.cn)

J. Lei, High Altitude Observatory, National Center for Atmospheric Research, Boulder, CO 80301, USA. (leijh@ucar.edu)

M. P. Sulzer, Arecibo Observatory, National Astronomy and Ionosphere Center, Cornell University, Arecibo, PR 00613-0995, USA. (sulzer@naic.edu)

M.-L. Zhang, Institute of Geology and Geophysics, Chinese Academy of Sciences, Beijing 100029, China. (zhangml@mail.iggcas.ac.cn)